5134 *Biochemistry* **2010,** *49,* 5134–5142
DOI: 10.1021/bi100246u

BIOCHEMISTRY
including biophysical chemistry & molecular biology
Article

Solution Structure of GxTX-1E, a High-Affinity Tarantula Toxin Interacting with Voltage Sensors in Kv2.1 Potassium Channels[†,‡]

Seungkyu Lee,[§] Mirela Milescu,[∥] Hyun Ho Jung,[§] Ju Yeon Lee,[§] Chan Hyung Bae,[§] Chul Won Lee,[⊥] Ha Hyung Kim,[@] Kenton J. Swartz,[∥] and Jae Il Kim*[,§]

[§]*Department of Life Science, Gwangju Institute of Science and Technology, Gwangju 500-712, South Korea,* [∥]*Molecular Physiology and Biophysics Section, National Institute of Neurological Disorders and Stroke, National Institutes of Health, Bethesda, Maryland 20892,* [⊥]*Department of Molecular Biology and The Skaggs Institute for Chemical Biology, The Scripps Research Institute, 10550 North Torrey Pines Road, La Jolla, California 92037, and* [@]*College of Pharmacy, Chung-Ang University, Seoul 156-756, South Korea*

Received February 17, 2010; Revised Manuscript Received May 28, 2010

ABSTRACT: GxTX-1E is a neurotoxin recently isolated from *Plesiophrictus guangxiensis* venom that inhibits the Kv2.1 channel in pancreatic β-cells. The sequence of the toxin is related to those of previously studied tarantula toxins that interact with the voltage sensors in Kv channels, and GxTX-1E interacts with the Kv2.1 channel with unusually high affinity, making it particularly useful for structural and mechanistic studies. Here we determined the three-dimensional solution structure of GxTX-1E using NMR spectroscopy and compared it to that of several related tarantula toxins. The molecular structure of GxTX-1E is similar to those of tarantula toxins that target voltage sensors in Kv channels in that it contains an ICK motif, composed of β-strands, and contains a prominent cluster of solvent-exposed hydrophobic residues surrounded by polar residues. When compared with the structure of SGTx1, a toxin for which mutagenesis data are available, the residue compositions of the two toxins are distinct in regions that are critical for activity, suggesting that their modes of binding to voltage sensors may be different. Interestingly, the structural architecture of GxTX-1E is also similar to that of JZTX-III, a tarantula toxin that interacts with Kv2.1 with low affinity. The most striking structural differences between GxTX-1E and JZTX-III are found in the orientation between the first and second cysteine loops and the C-terminal region of the toxins, suggesting that these regions of GxTX-1E are responsible for its high affinity.

Voltage-activated ion channels are used by excitable cells to generate and propagate electrical signals. These crucial ion channels are comprised of two domains: a central pore domain that is selective for either K^+, Na^+, or Ca^{2+} ions, surrounded by four voltage-sensing domains that move in response to changes in membrane voltage to open and close the pore (*1*, *2*). The venom from poison organisms such as scorpions and spiders contains peptide toxins that interact with these two types of domains. Charybdotoxin and related scorpion toxins, for example, bind to the outer vestibule of the pore to prevent ion conduction (*3*), whereas tarantula toxins such as HaTx,[1] SGTx, and VSTx interact with voltage sensors to modify gating of the channel (*4*). Both classes of toxins have been used extensively to probe the structure and functional mechanisms of voltage-activated ion channels (*5*−*12*).

Kv2.1 is an interesting voltage-activated K^+ channel that is widely expressed in the central nervous system and pancreatic β-cells, composing the delayed rectifier K^+ current and regulating excitability and Ca^{2+} influx during periods of repetitive high-frequency firing and glucose-dependent insulin secretion (*13*−*15*). Specific pore blockers of Kv2.1 have yet to be identified, although a variety of tarantula toxins such as HaTx1, SGTx1, and JZTX-III have been shown to bind to the channel's voltage-sensing domain and modify opening of the channel in response to membrane depolarization (*4*, *5*, *12*, *16*−*24*). Although these toxins have been useful in identifying structural motifs within voltage sensors that move at the protein−lipid interface (*5*, *7*, *12*, *25*−*27*), toxins with higher affinity and specificity would be particularly helpful for future structural, mechanistic, and physiological studies. The affinity of HaTx1 is relatively high (~100 nM) (*20*); however, its chemical synthesis and folding are technically challenging (*28*, *29*). SGTx1 and JZTX-III have relatively low affinity (2.7 μM and 430 nM, respectively) (*19*, *22*, *24*), and all three toxins also interact with voltage-activated Na^+ or Ca^{2+} channels (*6*, *23*, *24*, *30*).

GxTX-1E is a 36-amino acid peptide that was recently isolated from the venom of the tarantula *Plesiophrictus guangxiensis* and shown to inhibit outward K^+ channel currents in pancreatic β-cells, as well as hKv2.1 channels expressed in mammalian cells or *Xenopus* oocytes, in all cases with low nanomolar affinity (*31*, *32*). Saturation binding assays with the iodinated toxin also show that

[†]This research was supported by grants from the Brain Research Center of the 21st Century Frontier Research Program (M103KV010005-06K2201-00510), by the BioImaging Research Center at GIST, and by the Intramural Research Program of the National Institute of Neurological Disorders and Stroke, National Institutes of Health.

[‡]NMR assignment data and atomic coordinates of GxTX-1E have been deposited in BioMagResBank (entry 16960) and Protein Data Bank (entry 2WH9).

*To whom correspondence should be addressed: Department of Life Science, Room 106, Gwangju Institute of Science and Technology, Gwangju 500-712, Korea. Telephone: 82-62-715-2494. Fax: 82-62-715-2484. E-mail: jikim@gist.ac.kr.

[1]Abbreviations: Cl-HOBt, 6-chloro-1-hydroxybenzotriazole; DIC, 1,3-diisopropylcarbodiimide; DQF-COSY, double-quantum-filtered correlation spectroscopy; Fmoc, 9-fluorenylmethoxycarbonyl; HaTx, hanatoxin; ICK, inhibitory cystine knot; Kv, voltage-activated potassium channel; MALDI-TOF MS, matrix-assisted laser desorption ionization time-of-flight mass spectrometry; NOE, nuclear Overhauser effect; NOESY, NOE spectroscopy; NMR, nuclear magnetic resonance; PDB, Protein Data Bank; rms, root-mean-square; rmsd, root-mean-square deviation; RP-HPLC, reversed-phase high-performance liquid chromatography; TFA, trifluoroacetic acid; TOCSY, total correlation spectroscopy; TSP, trimethylsilyl-2,2,3,3-tetradeuteropropionic acid.

 Published on Web 05/28/2010

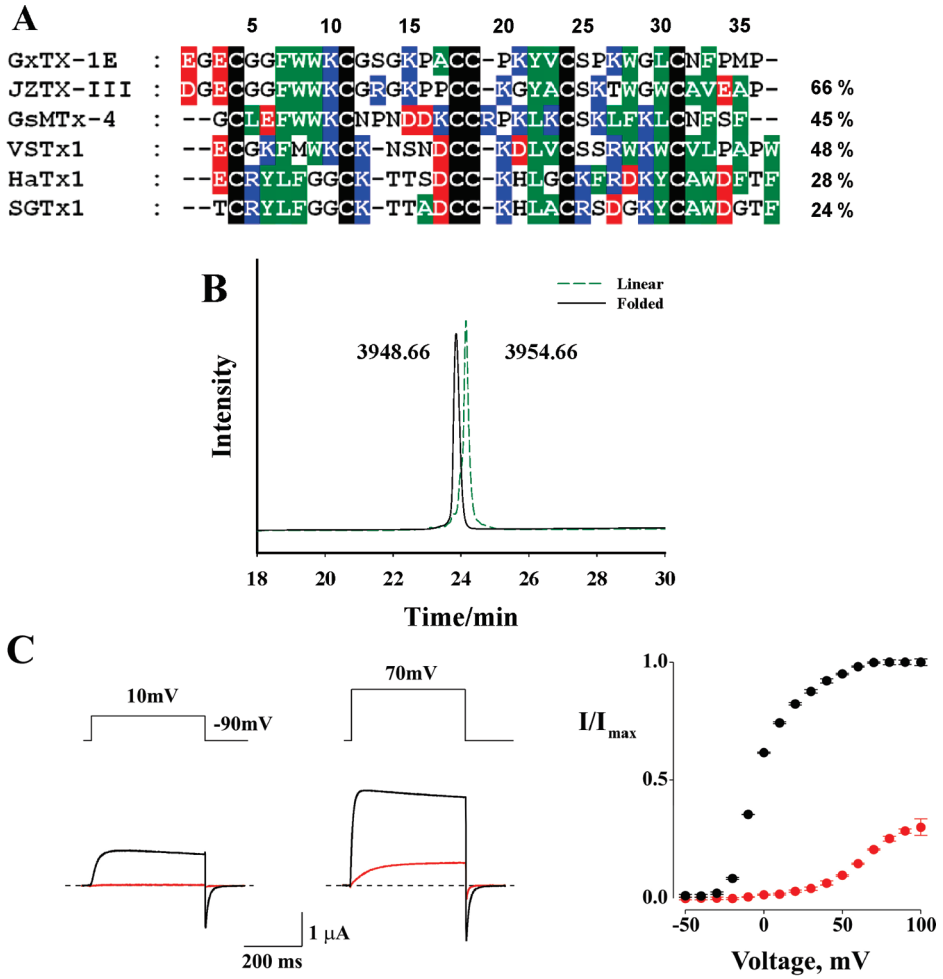

FIGURE 1: (A) Sequence alignment of GxTX-1E and homologous toxins. Red, blue, green, and black highlighting indicate acidic, basic, hydrophobic, and cysteine residues, respectively. The other residues are not colored. Numbers to the right are the percent similarity to GxTX-1E calculated by ClustalX. (B) RP-HPLC chromatogram of linear and folded GxTX-1E. The peptides were eluted with a linear gradient from 5 to 65% acetonitrile in water (0.1% TFA) over 30 min at a flow rate of 1 mL/min. (C) Voltage-activated potassium currents for the Kv2.1 channel recorded in the absence (black) or presence (red) of 100 nM GxTX-1E for various strength depolarizations (left). Voltage−activation relationships (right) were obtained using tail current measurements at −50 mV.

the toxin binds with high affinity to hKv2.1 channels (*33*). The sequence of GxTX-1E is similar to those of toxins known to interact with voltage sensors (Figure 1A), and electrophysiological studies show that the toxin inhibits Kv2.1 by modifying gating (*31*, *32*) and that mutations in the S3b-S4 paddle region of the voltage-sensing domain of Kv2.1 weaken toxin affinity (*34*). The promiscuous targeting of voltage sensors by tarantula toxins (*6*, *23*, *30*, *35*) does not appear to occur in the case of GxTX-1E, as the toxin has no effect on a wide range of voltage-activated K^+, Na^+, and Ca^{2+} channels (*31*, *32*). To provide a structural basis for future structural and mechanistic studies with GxTX-1E, we synthesized the toxin using solid-phase chemical methods and determined its solution structure using NMR.

MATERIALS AND METHODS

GxTX-1E Synthesis and Folding. The linear precursor of GxTX-1E was synthesized using Fmoc chemistry on Fmoc-Pro-Wang resin by an Applied Biosystems model 433A peptide synthesizer. A 4 mol excess of Fmoc amino acid, DIC, and Cl-HOBt were used for amino acid activation. The linear peptide was cleaved from resin by TFA for 4 h, in which phenol (7%), ethanedithiol (2.5%), thioanisole (5%), and water (5%) were used as scavengers. After cleavage, 15 mg of NH_4I and 20 μL of DMS per milliliter of TFA were reacted for 5 min to remove methionine oxidation. The crude peptide was precipitated in diethyl ether, followed by extraction with 20% (v/v) acetic acid, and diluted to a final concentration of 25 μM. Refolding of linear precursor was achieved at 4 °C for 3 days by air oxidation in 1 M guanidine-HCl, 0.1 M ammonium acetate, 2.5 mM reduced glutathione, and 0.25 mM oxidized glutathione (pH 8.0). The folding reaction was monitored with RP-HPLC, and the oxidized product was purified by ion-exchange chromatography with CM-cellulose (CM-52) and preparative RP-HPLC with a C18 silica column. The purity of the synthetic GxTX-1E was confirmed by analytical RP-HPLC and MALDI-TOF-MS measurements.

Electrophysiological Recording. The rKv2.1 Δ7 channel (*13*, *30*) was expressed in *Xenopus laevis* oocytes and studied using two-electrode voltage-clamp recording techniques (OC-725C, Warner Instruments) as previously described (*16*). Kv2.1 Δ7 contains seven mutations in the outer vestibule of the pore (T355S, K356G, A362D, S363A, I379M, Y380T, and K382V), rendering the channel sensitive to the pore-blocking toxin Agitoxin-2 and thus enabling the toxin to be used to subtract background conductances. Data were filtered at 1 kHz and digitized at 10 kHz. Microelectrode resistances were 0.1−1 MΩ when the electrodes were filled with 3 M KCl. For ionic current measurements, the external recording

solution contained 50 mM KCl, 50 mM NaCl, 5 mM HEPES, 1 mM $MgCl_2$, and 0.3 mM $CaCl_2$ (pH 7.6) with NaOH. All experiments were performed at room temperature (~22 °C). Conductance−voltage relationships were obtained from tail currents measured after a series of membrane depolarizations.

NMR Measurements. Synthetic GxTX-1E (20 mg) was dissolved in 500 μL of water containing 10% (v/v) ^2H_2O and finally adjusted to pH 3.5 and 6.0 with NaO^2H or ^2HCl. NMR experiments were conducted at 283, 300, and 310 K on a Bruker DRX 600 spectrometer. TOCSY spectra were recorded using a MLEV-17 pulse scheme (*36*) with isotropic mixing times of 80 ms. NOESY spectra were recorded with mixing times of 80, 150, and 250 ms. The two-dimensional NMR experiments included TOCSY and NOESY experiments and were conducted using the WATERGATE scheme for water suppression (*37*). DQF-COSY (*38*) spectra were recorded to obtain the constraints for the torsion angles. For the amide proton-exchange experiments, the lyophilized sample was dissolved in 99.96% ^2H_2O, and then a series of TOCSY experiments were performed on time scales of 2.5, 5, 7.5, 10, 12.5, 15, and 24 h at 300 K. Processing and analysis of the spectra were conducted using XWIN NMR and Sparky (*39*).

Structure Calculations. Peak lists of XEASY format for the NOESY spectra recorded with a mixing time of 250 ms at pH 3.5 and 310 K were generated and integrated using Sparky (*39*). For each disulfide bond, we used three standard upper limit distance constraints, S(i)−S(j), S(i)−C^{β}(j), and S(j)−C^{β}(i), with target values set to 2.04, 3.49, and 3.49 Å, respectively. The hydrogen bond acceptors for the slowly exchanged amide protons were identified via analysis of the preliminary calculated structures. The upper limit distance constraints of hydrogen bonds were used as target values of 2.0 Å for NH−O bonds and 3.0 Å for N−O bonds. The backbone NH−C^{α}H coupling constants were estimated from the DQF-COSY spectrum and were converted to backbone torsion angle φ constraints according to the following rules. For $^3J_{HN\alpha}$ values of < 5.5 Hz, the φ angle is constrained in the range of $-65 \pm 25°$; for $^3J_{HN\alpha}$ values of > 8.0 Hz, it is constrained in the range of $-120 \pm 40°$.

The three-dimensional structure of GxTX-1E was determined using the standard protocol of combined automated NOE assignment and the structure calculation of CYANA version 2.1 (*40*). Seven cycles of combined automated NOESY assignment and the structure calculation were followed by a final structure calculation. The structure calculations seeded in each cycle form 100 randomized structures, and the standard simulated annealing schedule was used (*41*). The 20 structures with the lowest final CYANA target function values were retained for analysis and passed to the next cycle. The 20 structures with the lowest final CYANA target function values were subjected to water refinement (*42*) and CNS energy minimization (*43*).

Evaluation of the Structure. The convergence of the calculated structures was evaluated in terms of the structural parameters. There were rms deviations from the experimental distance and dihedral constraints, from the energetic statistics, and from the idealized geometry. The 20 structures were analyzed or visualized using PROCHECK_NMR (*44*), PROMOTIF (*45*), MOLMOL (*46*), and PYMOL. The distributions of backbone dihedral angles in the final converged structure were evaluated by representation of the Ramachandran dihedral pattern, which indicated deviations from the allowed φ and ψ angle limits. The degrees of angular variation among the converged structures were further assessed using an angular order parameter. The solvent accessible surface areas for the side chains of amino acid residues were calculated with a solvent radius of 1.4 Å.

RESULTS

Synthesis and Oxidative Folding of GxTX-1E. A linear precursor of GxTX-1E was synthesized by the solid-phase methodology using Fmoc chemistry. During the cleavage reaction, NH_4I and DMS were added to prevent methionine oxidation. Controlled air oxidation of the linear precursor yielded satisfactory amounts of correctly folded GxTX-1E on RP-HPLC. The crude cyclized GxTX-1E was purified using ion-exchange chromatography and preparative RP-HPLC (Figure 1B), and MALDI-TOF analysis of synthetic GxTX-1E showed the expected molecular mass (3948.66 Da). Electrophysiological characterization of the synthetic toxin shows that it has robust activity against the Kv2.1 channel (Figure 1C). At a concentration of 100 nM, synthetic GxTX-1E completely inhibits opening of the Kv2.1 channel at negative membrane voltages and dramatically shifts channel activation to positive voltages, consistent with previous results (*32*, *33*).

NMR Analysis. Complete signal assignments for all of the observed protons in GxTX-1E were determined using ^{1}H 2D NMR methods following the standard protocols established by Wüthrich (*47*). Identification of the amino acid spin system was based on scalar coupling patterns observed in DQF-COSY and TOCSY experiments, complemented by the results of NOESY measurements. The identified spin systems were ordered along the primary structure of GxTX-1E through interresidue sequential NOEs observed on the NOESY spectrum. Some peaks displayed large chemical shifts compared to what would be expected for residues in a random coil. The NH peak of C19 (10.639 ppm) showed a downfield shift, which is typical of the fourth cysteine in an ICK motif peptide. In contrast, the C^{α}H (3.182 ppm) peak of F7, the N_1H (9.533 ppm) and C^{α}H (3.864 ppm) peaks of W8, the NH (7.652 ppm) peak of K21, and the NH (6.834 ppm) peak of L30 showed upfield shifts compared to those of random coils (Table S1 of the Supporting Information). All proline residues (P16, P20, P26, P34, and P36) take the trans configuration based on the observation of strong sequential NOE cross-peaks between the α proton of the residue prior to the proline and the δ protons of the proline.

The intensity of assigned NOEs, J coupling constants, slowly exchanging amide protons, and chemical shift index were interpreted in terms of the secondary structure of GxTX-1E (Figure 2). GxTX-1E contains three short β-strands consisting of residues 9−10, 23−24, and 30−32, which are arranged in an antiparallel fashion with several turns. The extent of the β-strands and their relative orientation were determined using strong sequential $d_{\alpha N}$, interstrand NH−NH and NH−C^{α}H connectivities, slowly exchanging amide protons (W9, V23, and S25), and large $^3J_{HN\alpha}$ coupling constants (W8, W9, Y22, V23, C24, G29, L30, and N32).

Calculation of the Solution Structure of GxTX-1E. The information from chemical shifts and NOE intensities was applied to CYANA calculation along with 14 dihedral angle constraints, 12 hydrogen bond constraints, and nine disulfide bond constraints. Of the 688 cross-peaks identified in the NOESY spectrum, 677 peaks were assigned using CYANA version 2.1. In the course of structure calculations for GxTX-1E, 465 NOE constraints were used, including 94 intraresidue, 172 sequential ($|i - j| = 1$), 61 medium-range ($1 < |i - j| < 5$), and 138 long-range ($|i - j| \geq 5$) NOE distance constraints. Observed NOE data were classified into four distance ranges, 1.8−2.7, 1.8−3.5, 1.8−5.0, and 1.8−6.0 Å, corresponding to strong, medium, weak, and very weak NOE values, respectively.

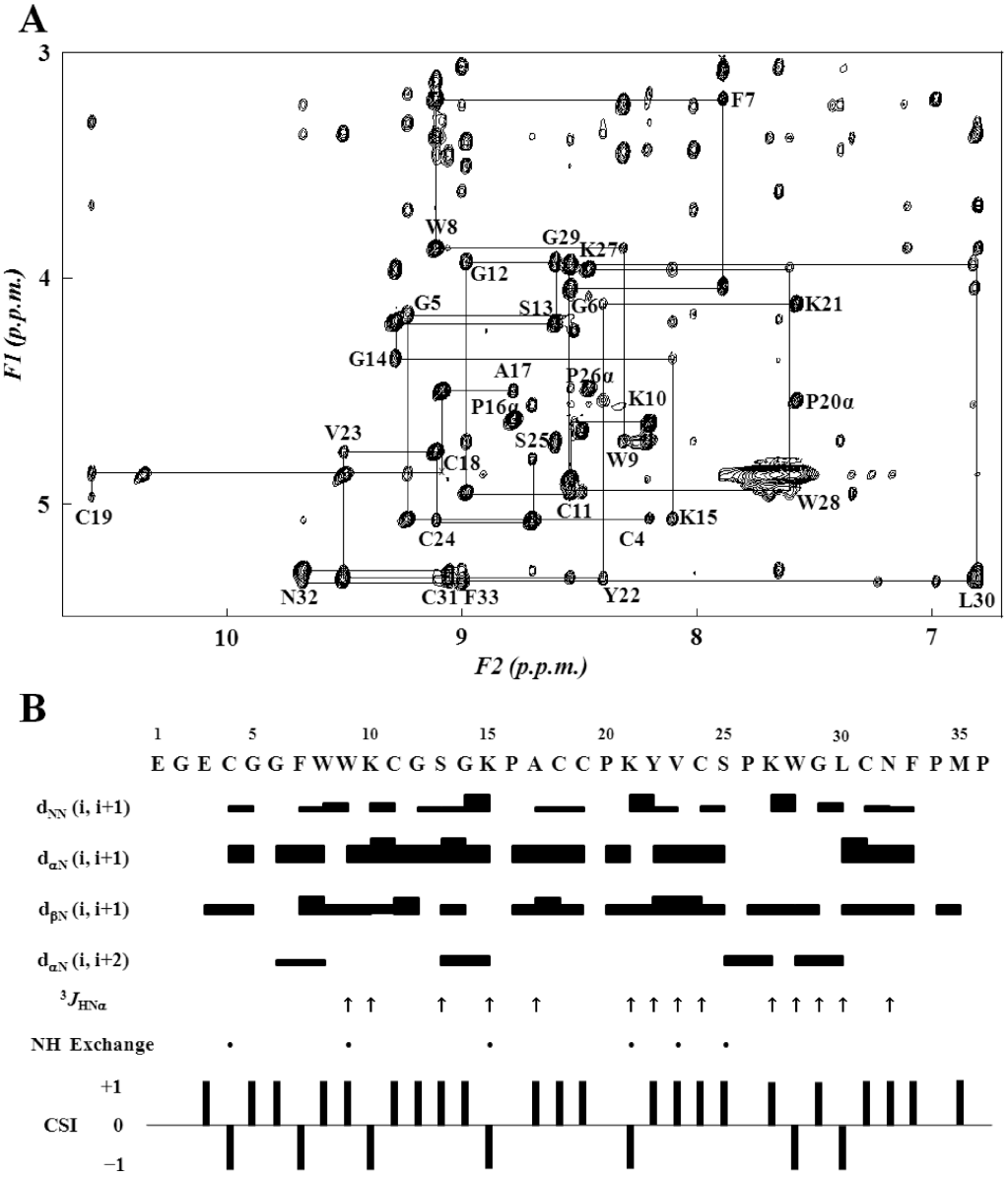

FIGURE 2: (A) Sequential $d_{\alpha N}(i,i+1)$ NOE connectivities for residues 4−33 in the NOESY spectrum observed with a mixing time of 250 ms. The $d_{\alpha N}$ connectivities of the proline residues are shown for P16 and A17, P20 and K21, and P26 and K27. Intraresidue NH−C^{α}H cross-peaks are labeled with the residue number by standard single-letter amino acid abbreviations. (B) Summary of the sequential and medium-range NOE connectivities, $^{3}J_{HN\alpha}$ coupling constants, and slowly exchanging backbone NH protons observed in GxTX-1E. These structural parameters were used for the sequence-specific assignments and the identification of secondary structure elements in GxTX-1E. Sequential and medium-range NOEs, d_{NN}, $d_{\alpha N}$, $d_{\beta N}$, and $d_{\alpha N}(i,i+2)$ are indicated by bars between two residues. The classification of NOEs as strong, medium, weak, or very weak is indicated by the height of the filled bars. Values of the $^{3}J_{HN\alpha}$ coupling constants are indicated with ↑ (> 8 Hz). Filled circles denote backbone amide protons that were still observed in the TOCSY spectra after 24 h in $^{2}H_{2}O$. The chemical shift index is indicated by a ternary index with values of −1, 0, and +1. Values of −1 and +1 indicate a shift deviation from the random-coil value of greater than 0.1 ppm upfield and downfield, respectively, and those within the range of random-coil values are indicated by 0.

The 12 hydrogen bond constraints from amide proton-exchange experiments and the NOE spectrum were as follows: W9(NH)−C31(CO), W9(CO)−C31(NH), C11(NH)−G29(CO), V23(NH)−N32(CO), V23(CO)−N32(NH), and S25(NH)−L30(CO). The disulfide bonds (C4−C19, C11−C24, and C18−C31) were assigned on the basis of sequence homology (*19*, *25*, *29*, *48*, *49*), and the structure of GxTX-1E with disulfide bond constraints was calculated. A family of 20 structures was acquired from CYANA calculations, and subsequent water refinement and energy minimization using CNS gave the final structure whose statistics are summarized in Table 1. The structure and its statistics of GxTX-1E without disulfide bond constraints are also summarized in Figure S1 and Table S2 of the Supporting Information.

Except for the N-terminal (E1 and G2) and C-terminal (M35 and P36) residues, the average pairwise rms deviation between the 20 final structures was 0.48 ± 0.12 Å for backbone atoms and 1.12 ± 0.21 Å for all heavy atoms. Figure 3 shows the atomic rms deviations and the angular order parameters for φ and ψ torsion angles as a function of residue number. Interestingly, the atomic rms deviations of the backbone for G14, P16, P20, and P26 are between 1.0 and 1.4 Å, indicating that these regions of the toxin are less defined because of the lack of the number of medium- and long-range NOE constraints. In addition, the atomic rms deviations of all heavy atoms for four basic residues (K10, K15, K21, and K27) and one hydrophobic residue (F33) show rmsd values greater than 1.5 Å. The angular order parameters for most

Table 1: Structural Statistics for the Final 20 Structures of GxTX-1E

rms deviation from experimental distance constraints (Å) (486)[a]	0.003 ± 0.0001
rms deviation from experimental dihedral constraints (deg) (14)[a]	0.022 ± 0.0021
energetic statistics (kcal/mol)[b]	
total energy	20.5658 ± 0.2564
F_{NOE}	0.3623 ± 0.0285
F_{tor}	0.0010 ± 0.0002
F_{repel}	3.0706 ± 0.0943
rms deviation from idealized geometry	
bonds (Å)	0.0017 ± 0.0001
angles (deg)	0.3304 ± 0.0015
impropers (deg)	0.0812 ± 0.0013
Ramachandran analysis[c]	
most favored regions (%)	73.1
additionally allowed regions (%)	26.9
generously allowed regions (%)	0.0
disallowed regions (%)	0.0
average rms deviations (Å) (residues 3−34)	
backbone (N, C^{α}, C)	0.48 ± 0.12
all heavy atoms	1.12 ± 0.21

[a]The numbers of experimental constraints used in each calculation are given in parentheses. [b]F_{NOE}, F_{tor}, and F_{repel} are the energies related to the NOE violations, the torsion angle violations, and the van der Waals repulsion term, respectively. The values of the force constants used for these terms are the standard values as depicted in the CNS 1.2 manual. [c]PROCHECK_NMR was used to assess the stereochemical quality of the structures.

residues from C4 to F33, except for the N- and C-terminal residues, show high S values (> 0.95), indicating that the backbone structures are well-defined. Analysis of the structures by PROCHECK shows that 73.1% of the residues are in the most favored region and 26.9% of the residues are in additionally allowed regions of the Ramachandran plot.

Molecular Structures. Figure 4A shows the best-fit superposition of the backbone atoms (N, C^{α}, and C) for the 20 converged structures. Analysis of the 20 converged structures indicates that the molecular structure of GxTX-1E (PDB entry 2WH9) consists of three short β-strands, four β-turns, and the disordered N- and C-terminal segments. The three β-strands are formed by W9−K10 (β-strand I), V23−C24 (β-strand II), and L30−N32 (β-strand III). The four β-turns involve G6−W9 (type IV), G12−K15 (type IV), C19−Y22 (type I), and S25−W28 (type IV). The average dihedral angles for residues at positions $i + 1$ and $i + 2$ of these β-turns are as follows: $\varphi_{i+1} = -70°$ and $\psi_{i+1} = -26°$ for F7, and $\varphi_{i+2} = -159°$ and $\psi_{i+2} = 78°$ for W8; $\varphi_{i+1} = -80°$ and $\psi_{i+1} = 92°$ for S13, and $\varphi_{i+2} = 121°$ and $\psi_{i+2} = 18°$ for G14; $\varphi_{i+1} = -59°$ and $\psi_{i+1} = -21°$ for P20, and $\varphi_{i+2} = -89°$ and $\psi_{i+2} = -33°$ for K21; $\varphi_{i+1} = -71°$ and $\psi_{i+1} = -34°$ for P26, and $\varphi_{i+2} = -82°$ and $\psi_{i+2} = -47°$ for K27. The first β-turn, as numbered from the N-terminus, presents in the loop (residues 3−9) between the N-terminal segment and β-strand I, and the second and third β-turns present in the external long loop (residues 12−22) between β-strands I and II. Interestingly, the backbone amide proton of K15 in the second β-turn shows unusually slow exchange rates in H−^{2}H exchange experiments, although K15 is highly exposed to solvent, indicating the formation of hydrogen bonds with the CO group of G12. The fourth β-turn connects β-strands II and III that form a 4:6 class hairpin motif (*50*), indicating that a single hydrogen bond is formed between the terminal NH group (S25) of β-strand II and the first CO group (L30) of β-strand III. Three disulfide bonds of GxTX-1E are well-defined (Figure 4A) and match an ICK motif (*51*, *52*). The disulfide bond between C11 and C24 interconnects β-strands I and II, while the disulfide bonds between C4 and C19 and between C18 and C31 connect the external long loop with the N-terminal region and β-strand III, respectively. The C4−C19 disulfide bond is categorized as a right-handed hook, and C11−C24 and C18−C31 disulfide bonds belong to a right-handed spiral and a left-handed spiral, respectively (*53*).

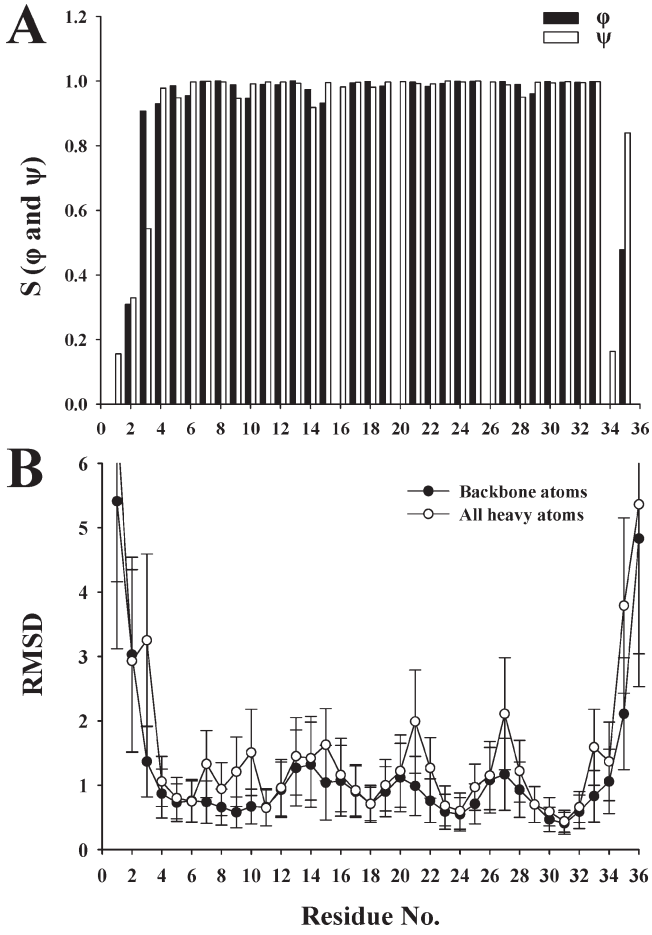

FIGURE 3: (A) Angular order parameters for φ and ψ angles calculated from the 20 converged structures. The S values define the two limits of an exactly defined angle ($S = 1$) and a completely random distribution of the angle ($S = 0$). (B) Distribution of the rmsds of backbone atoms (N, C^{α}, and C) and all heavy atoms for the 20 converged structures.

Surface Profile of GxTX-1E. On the surface of GxTX-1E are two negatively charged residues (E1 and E3), four positively charged residues (K10, K15, K21, and K27), and eight hydrophobic residues (F7, W8, W9, A17, V23, W28, F33, and M35) that exhibit solvent accessibilities of more than 20%. Interestingly, the six aromatic residues (F7, W8, W9, Y22, W28, and F33), along with one aliphatic residue (L30), cluster together on one face of the structure (Figure 4B). Of these residues, residue L30 of β-strand III is largely buried, showing low solvent accessibility (3.1%). The area of the exposed hydrophobic regions is 754.01/3233.745 Å^2 (F7, W8, W9, Y22, W28, L30, and F33). All negatively and positively charged residues surround the hydrophobic cluster, giving a net charge of +2. As a result of this cluster, the C^{α}H and NH peaks of F7, the N_1H and C^{α}H peaks of W8, and the NH peak of L30 were observed at unusual upfield positions, even though β-strand conformations have the tendency to cause downfield shifts, indicating that this phenomenon might result from an electromagnetic shielding effect of ring currents in clustered aromatic residues.

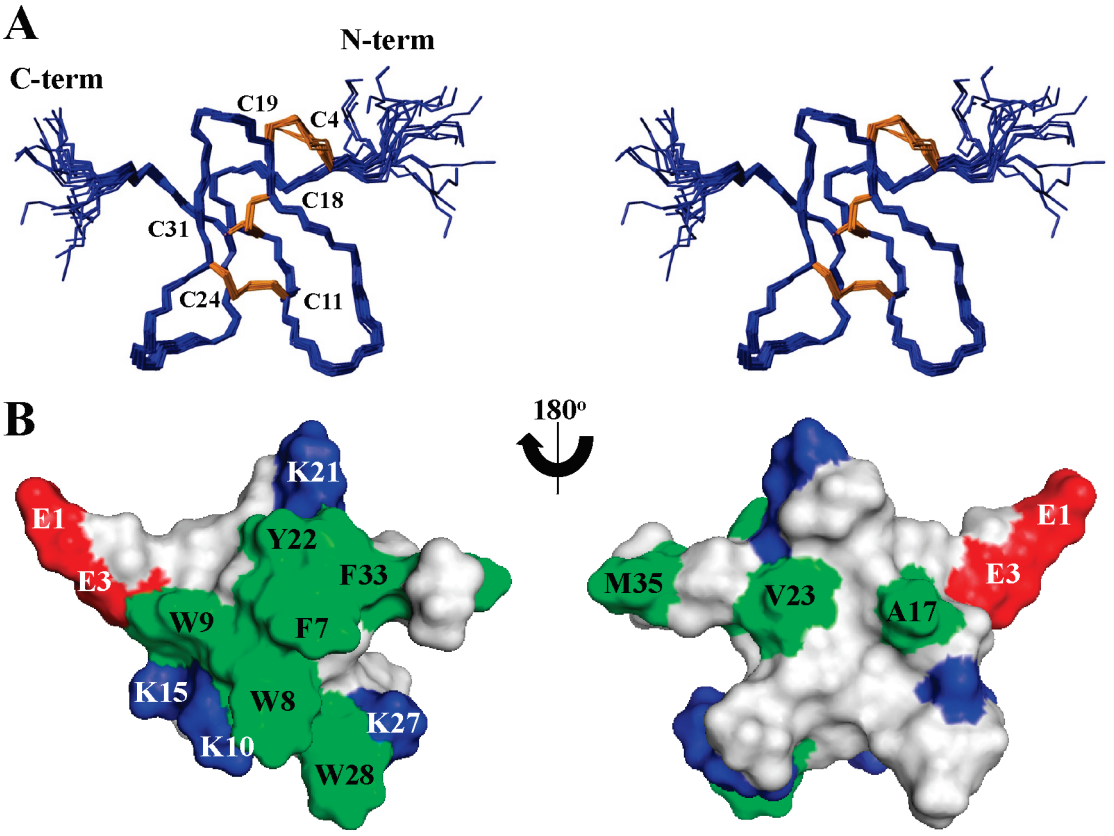

FIGURE 4: (A) Stereopairs of backbone atoms (N, C^{α}, and C) for the 20 converged structures of GxTX-1E. These are the results of the best-fit superposition of the backbone atoms in the central part (residues 3−34) of the molecule. Disulfide bonds are colored brown. (B) Surface profile of GxTX-1E. The left and right structures are rotated 180° relative to one another about a vertical axis. Hydrophobic, basic, and acidic residues are colored green, blue, and red, respectively. The other residues are colored white.

DISCUSSION

The NMR structure of GxTX-1E presented here shows that the toxin has a variety of features in common with previously studied tarantula toxins of related amino acid sequence (Figure 1A). One face of the toxin is amphipathic, containing a large cluster of solvent-exposed hydrophobic residues that is surrounded by basic and acidic residues, and the structure of the toxin is stabilized by disulfide bonds in an ICK motif (Figure 4). All of these features have been observed in structures of HaTx1 (*29*), SGTx1 (*48*), VSTx1 (*25*), and JZTX-III (*19*), members of a family of toxins that interact with the voltage-sensing domains in Kv channels, as well as for GsMTx-4 (*54*), a tarantula toxin that inhibits stretch-activated cation channels (*55*). All of these toxins can partition effectively into lipid membranes (*7*, *12*, *26*, *34*, *55*), explaining the conserved amphipathic character observed in their structures. Those toxins that target Kv channels are thought to bind to the channel from a place within the membrane (*5*−, *7*, *12*, *16*−, *18*, *21*, *26*, *34*), whereas GsMTx-4 is thought to inhibit the channel by perturbing interactions between the membrane and the channel (*56*). Mutagenesis studies on SGTx1 suggest that the amphipathic surface of the toxin is crucial for interacting with the membrane, as well as for binding to the channel (*26*, *22*).

Closer examination of the GxTX-1E structure in the context of mutagenesis studies on SGTx1 reveals several interesting differences between these two toxins. First, the distribution of acidic and basic residues relative to the hydrophobic cluster is different for the two toxins. GxTX-1E has two acidic residues on its N-terminus (E1 and E3), a feature not seen in SGTx1, and SGTx1 contains two acidic residues (D24 and D31) on the other opposite side of the toxin (Figure 5). Mutation of D24 in SGTx1 has pronounced effects on toxin affinity, and naturally occurring conservative substitution at E1 (E to D) alters GxTX-1E affinity (*32*), suggesting that these acidic regions may be important. Second, the residues in SGTx1 that are most important for toxin−channel interactions are not conserved in GxTX-1E. In SGTx1, mutations of R3, L5, F6, R22, and W30 weaken the toxin−channel interaction disproportionately compared to their effects on toxin−membrane interactions (*22*, *26*), making them candidates for involvement in the protein−protein interface between the toxin and channel. In GxTX-1E, basic residues are not found in positions corresponding to R3 and R22, and the position corresponding to R3 is actually occupied by an acidic residue (E3). Residue F6 in SGTx1 occupies a position similar to that of W8 in GxTX-1E, and W30 in SGTx1 occupies a position similar to that of F33 in GxTX-1E. Although these aromatic residues may play similarly important roles in the two toxins, their detailed spatial arrangements are clearly different. This comparison between GxTX-1E and SGTx1 raises the possibility that these two types of tarantula toxins interact with voltage sensors in ways that are distinct. This inference is supported by scanning mutagenesis of the S3b-S4 paddle region of Kv2.1, where many mutations that weaken toxin affinity are unique between GxTX-1E (*34*) and HaTx (*17*, *18*, *21*), a toxin that is very closely related to SGTx1.

Comparison of the structures of GxTX-1E and JZTX-III provides clues about the higher affinity and selectivity of GxTX-1E (*32*), because the two toxins have similar sequences, yet JZTX-III has a relatively low affinity for Kv2.1 (*24*) and also interacts with voltage-activated Na^{+} channels (*23*). In the three-dimensional structure, the overall folds of the two toxins are

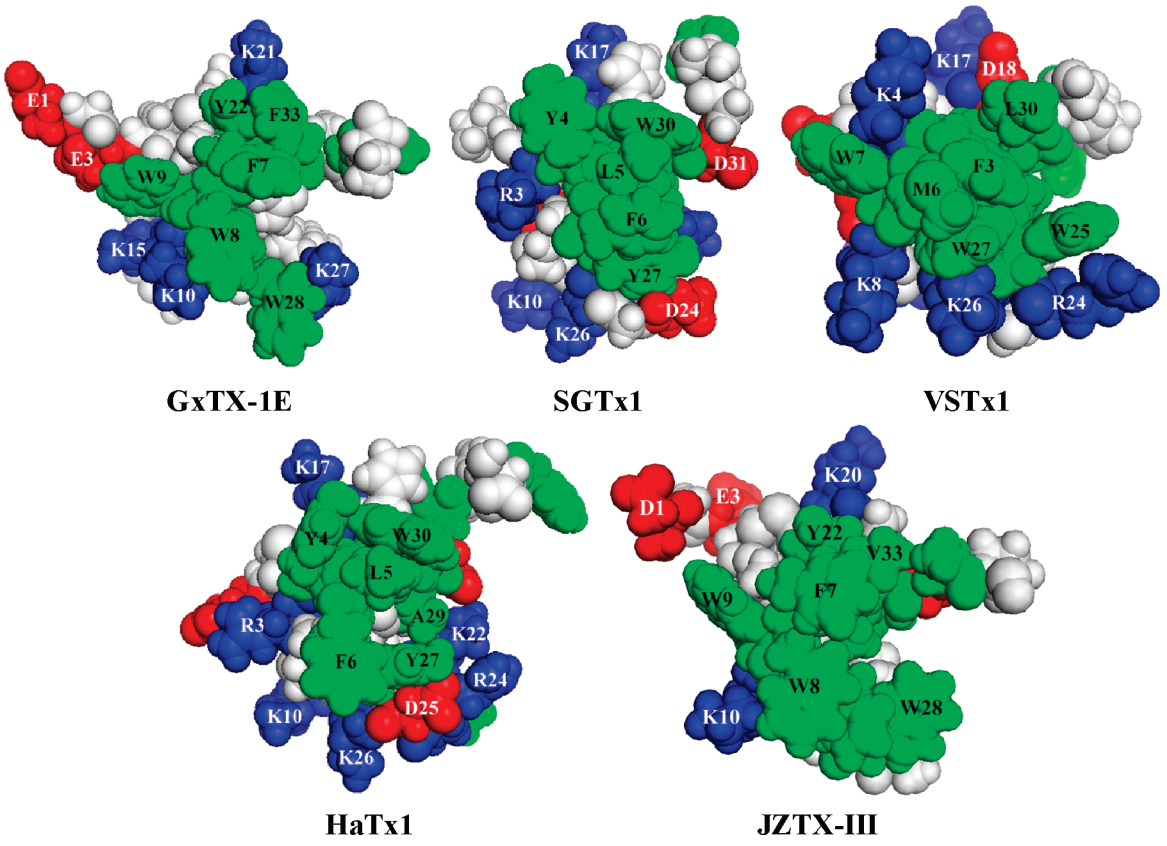

FIGURE 5: Space-filling models of GxTX-1E, SGTx1, VSTx1, HaTx1, and JZTX-III. Hydrophobic, basic, and acidic residues are colored green, blue, and red, respectively. The atomic coordinates of SGTx1, VSTx1, HaTx1, and JZTX-III were obtained from PDB entries 1LA4, 1S6X, 1D1H, and 2I1T, respectively.

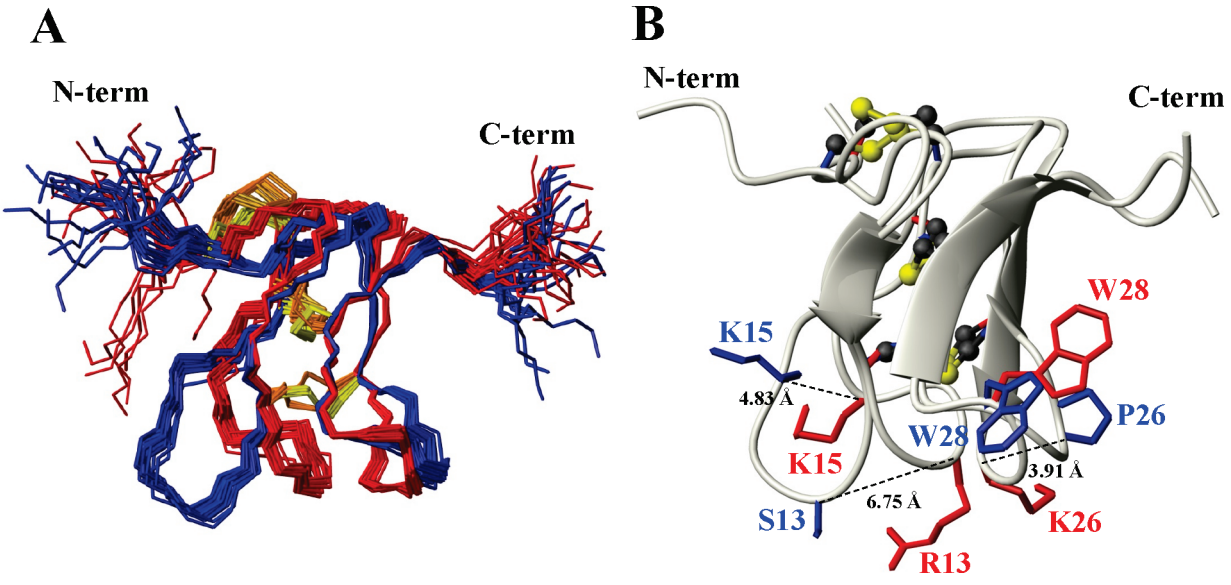

FIGURE 6: (A) Superposition of 20 GxTX-1E structures (blue) with 20 JZTX-III structures (red). The structures were fit on three β-strands of two toxins. Disulfide bonds of GxTX-1E and JZTX-III are colored yellow and dark orange, respectively. (B) Different spatial distributions for particular residues in the second and fourth turns of GxTX-1E and JZTX-III with the lowest-energy structures. The side chains of GxTX-1E and JZTX-III are colored blue and red, respectively, on the ivory backbones. Disulfide bonds are colored yellow. The C^{α} atom distances between S13, K15, and P26 of GxTX-1E and R13, K15, and K26 of JZTX-III, respectively, are depicted. The atomic coordinates of JZTX-III were obtained from PDB entry 2I1T.

similar, and both toxins contain a prominent cluster of hydrophobic residues that is surrounded by basic and acidic residues (Figure 5). Interestingly, however, the orientation between the first (C4−C18) and second cysteine loops (C19−C31) in JZTX-III is somewhat different from what is observed in GxTX-1E. In JZTX-III, the second and fourth turns are tilted against each other compared to those in GxTX-1E, which is based on NOE correlation peaks between the NH group of K26 and the $C^{\alpha}H$, $C^{\gamma}H_2$, and $C^{\delta}H_2$ groups of R13 due to probably juxtaposed prolines (P16 and P17) in JZTX-III (*19*). Four residues in these

two loops in GxTX-1E (S13, K15, P26, and W28) occupy considerably different spatial positions compared with the corresponding residues (R13, K15, K26, and W28) in JZTX-III. In comparison with the lowest-energy structures that are fitted on three β-strands, the C^{α} atom distances between S13, K15, and P26 for GxTX-1E and R13, K15, and K26 for JZTX-III are 6.75, 4.83, and 3.91 Å, respectively. Interestingly, the C^{α} atoms of W28 in both toxins have similar positions in their backbone coordinates, but the orientation of indole side chains is inverted against each other (Figure 6). In addition, the most notable sequence differences between the two toxins are in the C-terminal regions, beginning with L30 in GxTX-1E (which is W30 in JZTX-III), in which most residues are radically different between the two toxins (Figure 1A). It will be interesting to undertake further structural and functional studies with mutants and chimeras of these two toxins to explore how these localized structural differences influence affinity and selectivity.

In conclusion, the NMR structure of GxTX-1E will be useful in guiding future studies aimed at exploring how tarantula toxins interact with voltage sensors in Kv channels. GxTX-1E is easier to synthesize than many other related toxins (e.g., HaTx1) (*29*), and its higher affinity will enable double mutant cycle analysis (*57*, *58*) to be used in the identification of interacting residues at the protein−protein interface between the toxin and channel. The high affinity of GxTX-1E may also make the toxin particularly useful for stabilizing Kv channels in a resting/closed state for structural studies. The Kv1.2/2.1 paddle chimera channel containing the paddle motif of Kv2.1 would make a particularly attractive candidate for crystallization trials with GxTX-1E, as a structure of the open state of this channel has already been determined (*1*) and GxTX-1E interacts with the paddle motif in Kv2.1 (*34*). In all of these applications, the structural information provided here for GxTX-1E will be valuable.

SUPPORTING INFORMATION AVAILABLE

Chemical shifts of ^{1}H resonances of GxTX-1E and structures of GxTX-1E calculated with and without disulfide bond constraints. This material is available free of charge via the Internet at http://pubs.acs.org.

REFERENCES

1. Long, S. B., Tao, X., Campbell, E. B., and MacKinnon, R. (2007) Atomic structure of a voltage-dependent K^+ channel in a lipid membrane-like environment. *Nature 450*, 376–382.
2. Swartz, K. J. (2008) Sensing voltage across lipid membranes. *Nature 456*, 891–897.
3. Miller, C. (1995) The charybdotoxin family of K^+ channel-blocking peptides. *Neuron 15*, 5–10.
4. Swartz, K. J. (2007) Tarantula toxins interacting with voltage sensors in potassium channels. *Toxicon 49*, 213–230.
5. Alabi, A. A., Bahamonde, M. I., Jung, H. J., Kim, J. I., and Swartz, K. J. (2007) Portability of paddle motif function and pharmacology in voltage sensors. *Nature 450*, 370–375.
6. Bosmans, F., Martin-Eauclaire, M. F., and Swartz, K. J. (2008) Deconstructing voltage sensor function and pharmacology in sodium channels. *Nature 456*, 202–208.
7. Lee, S. Y., and MacKinnon, R. (2004) A membrane-access mechanism of ion channel inhibition by voltage sensor toxins from spider venom. *Nature 430*, 232–235.
8. MacKinnon, R. (1991) Determination of the subunit stoichiometry of a voltage-activated potassium channel. *Nature 350*, 232–235.
9. MacKinnon, R., Cohen, S. L., Kuo, A., Lee, A., and Chait, B. T. (1998) Structural conservation in prokaryotic and eukaryotic potassium channels. *Science 280*, 106–109.
10. MacKinnon, R., and Miller, C. (1989) Mutant potassium channels with altered binding of charybdotoxin, a pore-blocking peptide inhibitor. *Science 245*, 1382–1385.
11. Morin, T. J., and Kobertz, W. R. (2008) Counting membrane-embedded KCNE β-subunits in functioning K^+ channel complexes. *Proc. Natl. Acad. Sci. U.S.A. 105*, 1478–1482.
12. Phillips, L. R., Milescu, M., Li-Smerin, Y., Mindell, J. A., Kim, J. I., and Swartz, K. J. (2005) Voltage-sensor activation with a tarantula toxin as cargo. *Nature 436*, 857–860.
13. Frech, G. C., VanDongen, A. M., Schuster, G., Brown, A. M., and Joho, R. H. (1989) A novel potassium channel with delayed rectifier properties isolated from rat brain by expression cloning. *Nature 340*, 642–645.
14. MacDonald, P. E., and Wheeler, M. B. (2003) Voltage-dependent K^+ channels in pancreatic beta cells: Role, regulation and potential as therapeutic targets. *Diabetologia 46*, 1046–1062.
15. Misonou, H., Mohapatra, D. P., and Trimmer, J. S. (2005) Kv2.1: A voltage-gated K^+ channel critical to dynamic control of neuronal excitability. *Neurotoxicology 26*, 743–752.
16. Lee, H. C., Wang, J. M., and Swartz, K. J. (2003) Interaction between extracellular Hanatoxin and the resting conformation of the voltage-sensor paddle in Kv channels. *Neuron 40*, 527–536.
17. Li-Smerin, Y., and Swartz, K. J. (2000) Localization and molecular determinants of the hanatoxin receptors on the voltage-sensing domain of a K^+ channel. *J. Gen. Physiol. 115*, 673–684.
18. Li-Smerin, Y., and Swartz, K. J. (2001) Helical structure of the COOH terminus of S3 and its contribution to the gating modifier toxin receptor in voltage-gated ion channels. *J. Gen. Physiol. 117*, 205–218.
19. Liao, Z., Yuan, C., Peng, K., Xiao, Y., and Liang, S. (2007) Solution structure of Jingzhaotoxin-III, a peptide toxin inhibiting both Nav1.5 and Kv2.1 channels. *Toxicon 50*, 135–143.
20. Swartz, K. J., and MacKinnon, R. (1997) Hanatoxin modifies the gating of a voltage-dependent K^+ channel through multiple binding sites. *Neuron 18*, 665–673.
21. Swartz, K. J., and MacKinnon, R. (1997) Mapping the receptor site for hanatoxin, a gating modifier of voltage-dependent K^+ channels. *Neuron 18*, 675–682.
22. Wang, J. M., Roh, S. H., Kim, S., Lee, C. W., Kim, J. I., and Swartz, K. J. (2004) Molecular surface of tarantula toxins interacting with voltage sensors in kv channels. *J. Gen. Physiol. 123*, 455–467.
23. Xiao, Y., Tang, J., Yang, Y., Wang, M., Hu, W., Xie, J., Zeng, X., and Liang, S. (2004) Jingzhaotoxin-III, a novel spider toxin inhibiting activation of voltage-gated sodium channel in rat cardiac myocytes. *J. Biol. Chem. 279*, 26220–26226.
24. Yuan, C., Yang, S., Liao, Z., and Liang, S. (2007) Effects and mechanism of Chinese tarantula toxins on the Kv2.1 potassium channels. *Biochem. Biophys. Res. Commun. 352*, 799–804.
25. Jung, H. J., Lee, J. Y., Kim, S., Eu, Y. J., Shin, S. Y., Milescu, M., Swartz, K. J., and Kim, J. I. (2005) Solution Structure and Lipid Membrane Partitioning of VSTx1, an Inhibitor of the KvAP Potassium Channel. *Biochemistry 44*, 6015–6023.
26. Milescu, M., Vobecky, J., Roh, S. H., Kim, S. H., Jung, H. J., Kim, J. I., and Swartz, K. J. (2007) Tarantula toxins interact with voltage sensors within lipid membranes. *J. Gen. Physiol. 130*, 497–511.
27. Tombola, F., Pathak, M. M., and Isacoff, E. Y. (2005) How far will you go to sense voltage? *Neuron 48*, 719–725.
28. Swartz, K. J., and MacKinnon, R. (1995) An inhibitor of the Kv2.1 potassium channel isolated from the venom of a Chilean tarantula. *Neuron 15*, 941–949.
29. Takahashi, H., Kim, J. I., Min, H. J., Sato, K., Swartz, K. J., and Shimada, I. (2000) Solution structure of hanatoxin1, a gating modifier of voltage-dependent K^+ channels: Common surface features of gating modifier toxins. *J. Mol. Biol. 297*, 771–780.
30. Li-Smerin, Y., and Swartz, K. J. (1998) Gating modifier toxins reveal a conserved structural motif in voltage-gated Ca^{2+} and K^+ channels. *Proc. Natl. Acad. Sci. U.S.A. 95*, 8585–8589.
31. Herrington, J. (2007) Gating modifier peptides as probes of pancreatic β-cell physiology. *Toxicon 49*, 231–238.
32. Herrington, J., Zhou, Y. P., Bugianesi, R. M., Dulski, P. M., Feng, Y., Warren, V. A., Smith, M. M., Kohler, M. G., Garsky, V. M., Sanchez, M., Wagner, M., Raphaelli, K., Banerjee, P., Ahaghotu, C., Wunderler, D., Priest, B. T., Mehl, J. T., Garcia, M. L., McManus, O. B., Kaczorowski, G. J., and Slaughter, R. S. (2006) Blockers of the delayed-rectifier potassium current in pancreatic β-cells enhance glucose-dependent insulin secretion. *Diabetes 55*, 1034–1042.
33. Schmalhoefer, W. A., Ratliff, K. S., Weinglass, A. B., Kaczorowski, G. J., Garcia, M. L., and Herrington, J. (2009) A Kv2.1 gating modifier binding assay suitable for high throughput screening. *Channels 3*, 1–11.
34. Milescu, M., Bosmans, F., Lee, S., Alabi, A. A., Kim, J. I., and Swartz, K. J. (2009) Interactions between lipids and voltage sensor

paddles detected with tarantula toxins. *Nat. Struct. Mol. Biol. 16*, 1080–1085.
35. Middleton, R. E., Warren, V. A., Kraus, R. L., Hwang, J. C., Liu, C. J., Dai, G., Brochu, R. M., Kohler, M. G., Gao, Y. D., Garsky, V. M., Bogusky, M. J., Mehl, J. T., Cohen, C. J., and Smith, M. M. (2002) Two tarantula peptides inhibit activation of multiple sodium channels. *Biochemistry 41*, 14734–14747.
36. Bax, A., and Davis, D. G. (1985) MLEV-17-Based Two-Dimensional Homonuclear Magnetization Transfer Spectroscopy. *J. Magn. Reson. 65*, 355–360.
37. Piotto, M., Saudek, V., and Sklenar, V. (1992) Gradient-tailored excitation for single-quantum NMR spectroscopy of aqueous solutions. *J. Biomol. NMR 2*, 661–665.
38. Rance, M., Sorensen, O. W., Bodenhausen, G., Wagner, G., Ernst, R. R., and Wuthrich, K. (1983) Improved spectral resolution in cosy ^{1}H NMR spectra of proteins via double quantum filtering. *Biochem. Biophys. Res. Commun. 117*, 479–485.
39. Goddard, T. D., and Kneller, D. G. (2004) SPARKY 3, University of California, San Francisco.
40. Guntert, P. (2004) Automated NMR structure calculation with CYANA. *Methods Mol. Biol. 278*, 353–378.
41. Herrmann, T., Guntert, P., and Wuthrich, K. (2002) Protein NMR structure determination with automated NOE assignment using the new software CANDID and the torsion angle dynamics algorithm DYANA. *J. Mol. Biol. 319*, 209–227.
42. Linge, J. P., Williams, M. A., Spronk, C. A., Bonvin, A. M., and Nilges, M. (2003) Refinement of protein structures in explicit solvent. *Proteins 50*, 496–506.
43. Brunger, A. T., Adams, P. D., Clore, G. M., DeLano, W. L., Gros, P., Grosse-Kunstleve, R. W., Jiang, J. S., Kuszewski, J., Nilges, M., Pannu, N. S., Read, R. J., Rice, L. M., Simonson, T., and Warren, G. L. (1998) Crystallography & NMR system: A new software suite for macromolecular structure determination. *Acta Crystallogr. D54*, 905–921.
44. Laskowski, R. A., Rullmannn, J. A., MacArthur, M. W., Kaptein, R., and Thornton, J. M. (1996) AQUA and PROCHECK-NMR: Programs for checking the quality of protein structures solved by NMR. *J. Biomol. NMR 8*, 477–486.
45. Hutchinson, E. G., and Thornton, J. M. (1996) PROMOTIF: A program to identify and analyze structural motifs in proteins. *Protein Sci. 5*, 212–220.
46. Koradi, R., Billeter, M., and Wuthrich, K. (1996) MOLMOL: A program for display and analysis of macromolecular structures. *J. Mol. Graphics 14*, 29–32, 51−55.
47. Wüthrich, K. (1986) NMR of proteins and nucleic acids, Wiley, New York.
48. Lee, C. W., Kim, S., Roh, S. H., Endoh, H., Kodera, Y., Maeda, T., Kohno, T., Wang, J. M., Swartz, K. J., and Kim, J. I. (2004) Solution Structure and Functional Characterization of SGTx1, a Modifier of Kv2.1 Channel Gating. *Biochemistry 43*, 890–897.
49. Takeuchi, K., Kim, J. I., Takahashi, H., Swartz, K., and Shimada, I. (2002) Solution structure of ω-grammotoxin SIA, a gating modifier of P/Q and N type calcium channels. *J. Mol. Biol. 321*, 517–526.
50. Sibanda, B. L., Blundell, T. L., and Thornton, J. M. (1989) Conformation of β-hairpins in protein structures. A systematic classification with applications to modeling by homology, electron density fitting and protein engineering. *J. Mol. Biol. 206*, 759–777.
51. Norton, R. S., and Pallaghy, P. K. (1998) The cystine knot structure of ion channel toxins and related polypeptides. *Toxicon 36*, 1573–1583.
52. Pallaghy, P. K., Nielsen, K. J., Craik, D. J., and Norton, R. S. (1994) A common structural motif incorporating a cystine knot and a triple-stranded β-sheet in toxic and inhibitory polypeptides. *Protein Sci. 3*, 1833–1839.
53. Richardson, J. S. (1981) The anatomy and taxonomy of protein structure. *Adv. Protein Chem. 34*, 167–339.
54. Oswald, R. E., Suchyna, T. M., McFeeters, R., Gottlieb, P., and Sachs, F. (2002) Solution structure of peptide toxins that block mechanosensitive ion channels. *J. Biol. Chem. 277*, 34443–34450.
55. Suchyna, T. M., Johnson, J. H., Hamer, K., Leykam, J. F., Gage, D. A., Clemo, H. F., Baumgarten, C. M., and Sachs, F. (2000) Identification of a peptide toxin from *Grammostola spatulata* spider venom that blocks cation-selective stretch-activated channels. *J. Gen. Physiol. 115*, 583–598.
56. Suchyna, T. M., Tape, S. E., Koeppe, R. E., II, Andersen, O. S., Sachs, F., and Gottlieb, P. A. (2004) Bilayer-dependent inhibition of mechanosensitive channels by neuroactive peptide enantiomers. *Nature 430*, 235–240.
57. Hidalgo, P., and MacKinnon, R. (1995) Revealing the architecture of a K^+ channel pore through mutant cycles with a peptide inhibitor. *Science 268*, 307–310.
58. Ranganathan, R., Lewis, J. H., and MacKinnon, R. (1996) Spatial localization of the K^+ channel selectivity filter by mutant cycle-based structure analysis. *Neuron 16*, 131–139.